TISSUE ENGINEERING: Part A
Volume 19, Number S1, 2014

DOI: 10.1089/ten.tea.2013.0357

Young Investigator Council Special Issue

Avidity-Controlled Delivery of Angiogenic Peptides from Injectable Molecular-Recognition Hydrogels

Widya Mulyasasmita, PhD,[1] Lei Cai, PhD,[2] Yuki Hori, PhD,[2] and Sarah C. Heilshorn, PhD[1,2]

Peptide mimics of growth factors represent an emerging class of therapeutic drugs due to high biological specificity and relative ease of synthesis. However, maintaining efficacious therapeutic dosage at the therapy site has proven challenging owing to poor intestinal permeability and short circulating half-lives in the blood stream. In this work, we present the affinity immobilization and controlled release of QK, a vascular endothelial growth factor (VEGF) mimetic peptide, from an injectable mixing-induced two-component hydrogel (MITCH). The MITCH system is crosslinked by reversible interactions between WW domains and complementary proline-rich peptide modules. Fusion of the QK peptide to either one or two units of the proline-rich sequence creates bifunctional peptide conjugates capable of specific binding to MITCH while preserving their angiogenic bioactivity. Presenting two repeats of the proline-rich sequence increases the binding enthalpy 2.5 times due to avidity effects. Mixing of the drug conjugates with MITCH components results in drug encapsulation and extended release at rates consistent with the affinity immobilization strength. Human umbilical vein endothelial cells (HUVECs) treated with the soluble drug conjugates exhibit morphogenetic events of VEGF receptor 2 signal transduction followed by cell migration and organization into networks characteristic of early angiogenesis. In a three-dimensional model where HUVECs were cultured as spheroids in a matrix of collagen and fibronectin, injection of drug-releasing MITCH resulted in significantly more cell outgrowth than drugs injected in saline. This ability to sustain local drug availability is ideal for therapeutic angiogenesis applications, where spatiotemporal control over drug distribution is a key requirement for clinical success.

Introduction

Recent years have witnessed clear trends in peptide drugs advancing into medical research endeavors, through clinical trials, and into the market.[1] Defined as polypeptides that contain fewer than 50 amino acids, peptides constitute a class of therapeutics distinct from small molecules and larger protein biologics, such as growth factors and antibodies. The attractiveness of peptides as drugs stems from the combined advantages of structural stability and lower cost of manufacturing afforded by small molecules with the specificity, potency, and low toxicity of protein biologics.[2] Concomitantly, advances in structural biology, proteomics, and peptide library screening methodologies have expedited the design and discovery of short amino acid sequences capable of recapitulating the biological functions of the parent full-length proteins.[3–5] Toward tissue engineering and regenerative medicine applications, peptides have been engineered to mimic a vast range of growth factors, including vascular endothelial growth factor[6] (VEGF), platelet-derived growth factor[7] (PDGF), nerve growth factor,[8] brain-derived neurotrophic factor,[9] and epidermal growth factor.[10]

Counteracting the therapeutic potential of peptide drugs is pharmacokinetic challenges associated with degradation, bioavailability, and metabolic clearance following administration.[11] Owing to the highly proteolytic environment of the stomach, as well as limited gastrointestinal absorption due to the large size (>500 Da) and hydrophilicity of peptides, delivery is almost exclusively through parenteral routes, especially via intravenous, subcutaneous, or intramuscular injection.[12] Once in the bloodstream, peptide drugs face rapid hepatic and renal clearance, resulting in short circulating half-lives.[13,14] Maintenance of dosage within therapeutic range necessitates frequent injections, calling into question pragmatic issues of reduced patient comfort, convenience, and compliance.[11]

Controlled delivery from hydrogels has emerged as a promising strategy to overcome challenges in peptide drug delivery.[15,16] Hydrogels are crosslinked polymeric networks whose high water content and porous structures make them ideal as drug-releasing reservoirs. Broadly, drug loading is achieved either through covalent immobilization via degradable linkers or noncovalent physical entrapment via simple encapsulation or affinity-based immobilization. Each of these mechanisms has tradeoffs. Covalent tethering to

Departments of [1]Bioengineering and [2]Materials Science and Engineering, Stanford University, Stanford, California.

hydrogel networks can potentially diminish peptide drug bioactivity, due to harsh chemical reaction conditions or fixation into inactive secondary conformations.[17,18] Physical entrapment often requires nonphysiological gelation triggers (e.g., changes in temperature or pH) that could expose peptide drugs to denaturing conditions. Also, release following simple encapsulation proceeds through Fickian diffusion, whose fast kinetics may sequester short peptides only momentarily. As an alternative approach, several groups have started exploring the use of noncovalent affinity immobilization to achieve slower release rates of biomacromolecules.[19–24] These systems typically require additional binding mediators that may be difficult to engineer into the drug carriers. One example is two-photon immobilization of barnase and streptavidin, followed by a binding step with the respective barstar- and biotin-growth factor fusions.[20] Mimicking growth factors' natural affinity to heparin, other systems have incorporated heparin as a binding mediator, either through direct heparin conjugation[21] or by covalent modification with heparin-binding peptides.[22] Because these systems involve multispecies complexations, extensive mathematical modeling is often needed to arrive at predictable release profiles.[23,24]

We previously reported a class of protein materials called MITCH, mixing-induced two-component hydrogels,[25–27] that upon simple mixing assemble into injectable physical hydrogels through specific crosslinking between complementary WW and proline-rich peptide domains (denoted as C and P, respectively). In this article, we further develop MITCH to design an injectable peptide drug delivery system that enables tailored and sustained peptide release. Release kinetics is controlled by using avidity effects to engineer the affinity immobilization strength. We demonstrate this immobilization and release strategy through the delivery of QK, a 15-amino-acid VEGF-mimetic peptide able to elicit angiogenic responses by binding and activating VEGF receptors.[6]

The stability of soluble QK peptide has been reported to be significantly better than the full-length VEGF protein. While VEGF-15 is rapidly degraded with a half-life of <15 min, QK is reported to degrade after 24 h in 50% human serum.[28] In soluble form, the QK peptide has been reported to demonstrate angiogenic bioactivity above a threshold concentration of about 1 pM.[6,28,29] The QK peptide has also demonstrated bioactivity across a broad range of concentrations (1 pM–100 μM) when presented as a substrate-bound peptide on collagen scaffolds via collagen-binding peptides,[30] on hydroxyapatite via binding of an osteocalcin sequence,[29] and on self-assembled monolayers via covalent immobilization.[31]

Keeping the MITCH network polymers unmodified, affinity immobilization is achieved simply by synthesizing a fusion of QK to a single proline-rich domain (P1), which acts as an affinity tag (Fig. 1). Solely by mixing with MITCH components, P1-QK conjugates are encapsulated in the network and docked onto pre-existing C domains without requiring nonphysiological gelation triggers. The release kinetics of P1-QK from MITCH was found to be significantly slower relative to unmodified QK. Further applying concepts of avidity, we demonstrate increased binding strength and even slower release by using a dimer of P domains (P2) as an alternate affinity tag. Both P1-QK and P2-QK fusion peptides maintained their angiogenic activity on human umbilical vein endothelial cells (HUVECs).

Materials and Methods

Protein synthesis and purification

The C7 and P9 protein polymers (Supplementary Fig. S1; Supplementary Data are available online at www.liebertpub.com/tea) were synthesized through recombinant expression in *Escherichia coli*, as previously reported.[25] Briefly, DNA sequences encoding the C7 and P9 proteins were cloned into the pET-15b (Novagen) and pJexpress414 (DNA 2.0) vectors, respectively, and transformed into the BL21*(DE3)pLysS *E. coli* host strain (Life Technologies). Protein was expressed by isopropyl β-D-1-thiogalactopyranoside (IPTG) induction and purified through the specific binding of polyhistidine tags to immobilized metal ion affinity chromatography columns, before buffer exchanging into phosphate-buffered saline (PBS) and concentrating by diafiltration across 30 kDa MWCO Amicon Ultracel-30K filter units (Millipore). Protein identity and purity were confirmed by gel electrophoresis (Supplementary Fig. S1). MALDI-TOF mass spectrometry

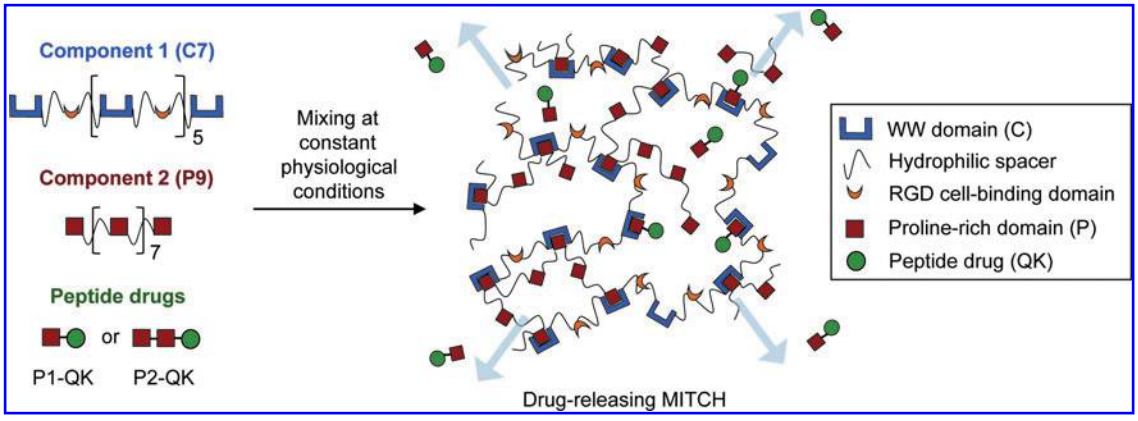

FIG. 1. Controlled release of peptide drugs by affinity immobilization to mixing-induced two-component hydrogels (MITCH). Conjugation of peptide drugs to P1 or P2 affinity tags followed by simple mixing with MITCH components, C7 and P9, results in drug encapsulation, binding immobilization, and subsequent slow release. Color images available online at www.liebertpub.com/tea

and amino acid compositional analysis were performed to provide additional confirmation (data not shown).

Peptide synthesis

QK, P1-QK, and P2-QK peptides were purchased through custom peptide synthesis from Genscript Corp. and confirmed to have purity of 92–98% by high-performance liquid chromatography.

Fluorescence recovery after photobleaching

Fluorescence recovery after photobleaching (FRAP) measurement was performed using peptides (QK, P1-QK, and P2-QK) conjugated with fluorescein isothiocyanate (FITC; Genscript). Peptides were individually mixed with MITCH (gel volume = 30 μL, concentration = 10% w/v) at a final peptide concentration of 4 mg/mL and the total fluorescence intensity was visualized at 37°C using a Leica TCS SP5 confocal microscope at low light intensity. Low melting point agarose (5% w/v) hydrogel (Invitrogen) was also used as an alternative hydrogel for FRAP measurement. Photobleaching was done by exposing a $100 \times 100\ \mu m^2$ spot in the field of view to high-intensity laser light. A series of images were taken every 3 s for 5 min to track the recovery of fluorescence. The resulting recovery profiles were modeled by Fickian diffusion according to a previously reported method[32] to calculate diffusivities of peptides in these hydrogels.

Bulk-release kinetics study

To facilitate spectrophotometric tracking, peptides (QK, P1-QK, and P2-QK) were fluorescently labeled with Alexa Fluor 488 5-SDP Ester (Invitrogen) for 1 h, according to the manufacturer's protocol. Reaction products were dialyzed (MWCO = 1.0 kDa) against PBS at 4°C over three buffer changes over a period of 12 h. To study peptide release, fluorescently labeled peptides were individually encapsulated in MITCH (gel volume = 40 μL, concentration = 10% w/v) by first mixing with P9 and subsequently with C7 in a circular silicone mold (diameter = 4 mm, height = 2 mm) within a 24-well plate ($n \geq 3$). The initial peptide concentration in the gel was 10 μM. The mixture was allowed to gel for 15 min at 37°C in a humidified incubator, after which 1.5 mL of PBS was added to each well. Release kinetics was followed by sampling and replenishing 100 μL of the PBS supernatant over a period of 21 days. To determine the amount of peptide remaining in the gel and still available for release, an endpoint analysis at day 21 was conducted by disrupting and solubilizing the entire gel. Bulk-release experiments of dextran were performed in an identical manner, using neutral Texas Red dextran (MW = 3, 40, or 70 kDa; Invitrogen) with an initial concentration of 10 μM in 40-μL gels ($n \geq 4$). Diffusivity constants of dextran in MITCH were obtained by fitting the cumulative release data to an equation that describes Fick's second law of diffusion from thin slabs.[33]

Isothermal titration calorimetry

The differential binding affinity of P1 and P2 peptides to C1 was studied by measuring enthalpy changes using a nano isothermal titration calorimetry (ITC) instrument (TA Instruments). All peptides were dissolved and dialyzed overnight (MWCO = 1.0 kDa) against PBS (pH 7.4) to ensure buffer matching. About 2 mM of C1 solution was loaded in the injection syringe and titrated into 0.2 mM P1 or P2 solution in the sample cell in a sequence of 16 injections of 3-μL volumes. Successive injections were delayed by 5 min to allow equilibration. All experiments were conducted at 25°C with constant stirring at 300 rpm. The NanoAnalyze software was used to transform raw heat against injection number into enthalpy change per mole of injectant against molar ratio. The integrated isotherms were then fitted to an independent-site model to obtain thermodynamic parameters of binding.

Far-UV circular dichroism spectroscopy

Circular dichroism (CD) spectra of peptides and peptide conjugates over a range of 195–250 nm were measured on a Jasco J-815 spectropolarimeter using a quartz cuvette with a pathlength of 10 mm. Peptide and peptide solution were dissolved at a concentration of 30 μM in PBS (pH 7.4), and spectral scanning was performed in triplicates at a speed of 100 nm/min and a data interval of 1 nm, averaged, and converted to mean residue ellipticity after background correction relative to PBS.

Cell culture and maintenance

HUVECs (Lonza) were cultured in EBM-2 endothelial basal medium with full EGM-2 bullet kit supplements (Lonza), and kept in a humidified, 5% CO_2 environment at 37°C with media changes every 2 days. Cells were passaged using TrypLE express (Invitrogen), and passages 2–7 were used in subsequent experiments.

VEGF receptor 2 phosphorylation assay by ELISA

HUVECs were grown to confluence in 100-mm culture dishes before they were starved in serum- and growth-factor-depleted EBM-2 medium for 24 h at 37°C and 5% CO_2. Cells were then rinsed with PBS and treated with (1) blank medium (serum and growth factor depleted), (2) blank medium with 1 μM P1-QK, or (3) blank medium with 1 μM P2-QK for 5 min at 37°C and 5% CO_2. The cells were then washed with PBS, trypsinized, transferred into conical tubes, and centrifuged into cell pellets. Cell lysis buffer (''Lysis Buffer #9'': 1% NP-40 Alternative, 20 mM Tris (pH 8.0), 137 mM NaCl, 10% glycerol, 2 mM EDTA, 1 mM activated sodium orthovanadate, 10 g/mL aprotinin, and 10 g/mL leupeptin; R&D Systems) was added to each of the lysates before centrifugation at 2000 *g* for 5 min. The supernatants were frozen at −80°C overnight, and quantified by ELISA ($n \geq 6$) according to the manufacturer's protocol (''Duo Set® IC, Human Phospho-VEGFR2/KDR''; R&D Systems).

Western blot

HUVECs were grown to confluence in six-well culture plates and starved in blank medium for 24 h at 37°C and 5% CO_2. Cells were then rinsed with PBS and treated with blank medium without or with supplementation of 1 μM of peptides (QK, P1-QK, or P2-QK) or 2 nM recombinant human VEGF 165 (R&D Systems) for 15 min at 37°C and 5% CO_2

($n \geq 4$). Cells were then rinsed with PBS twice and lysed using RIPA buffer (Cell Signaling Technology). Cell lysates were collected and centrifuged, and the supernatants were stored at $-80°C$. Immediately before the assay, protein concentrations were measured by NanoDrop 2000c Spectrophotometer (Thermo Scientific). Protein samples were separated by SDS-PAGE (45 μg per lane), and transferred onto PVDF Transfer Membrane (Thermo Scientific). Protein blots were blocked with 5% w/v nonfat milk in TBST buffer (Tris-buffered saline with 0.2% Tween 20) for 1 h at room temperature and probed with anti-pERK1/2 MAPK and anti-phospho-pERK1/2 MAPK antibodies (1:1000 dilution; Cell Signaling Technology) overnight at 4°C. The protein bands were visualized by horseradish-peroxidase-conjugated anti-rabbit secondary antibody (1:2000 dilution; Cell Signaling Technology) and chemiluminescence was detected on a BioRad Chemidoc instrument. Relative intensities of the chemiluminescence signal were quantified using the ImageJ software (National Institutes of Health).

Scratch wound healing assay

HUVECs were seeded in a 48-well tissue culture plate with a strip of silicone rubber ($10 \times 0.5 \times 0.5\ mm^3$, length × width × thickness) adhered to the bottom of each well. Cells were cultured until confluence in EBM-2 medium supplemented with 5% heat-inactivated fetal bovine serum (HI-FBS). The strip was removed to create a wound, and cells were incubated in medium without or with supplementation of 1 μM peptides (QK, P1-QK, or P2-QK) or 2 nM recombinant human VEGF 165 ($n \geq 4$). HUVECs were imaged at the same positions along the wound using phase-contrast microscopy (Leica TCS SP5, 10× objective) immediately upon strip removal and after 12 h. ImageJ software was used to quantify the area of cell migration into the wound. Wound closure is defined as the area invaded by cells 12 h after wounding relative to the original wound area.

HUVEC network assay within collagen sandwiches

HUVECs were starved in serum- and growth-factor-depleted EBM-2 medium (Lonza) overnight, trypsinized, and seeded in triplicate onto glass-bottomed circular silicone molds (diameter = 4 mm, height = 2 mm) precoated with 50 μL of polymerized rat tail collagen type I (BD Sciences; final concentration = 2 mg/mL). Cell-seeding density was 20,000 cells per mold. To allow attachment, cells were kept for 50 min at 37°C in a humidified incubator, after which an additional 50 μL of 2 mg/mL collagen was overlaid on the cell monolayer and left to polymerize for 40 min in the incubator to form a collagen-HUVEC-collagen ''sandwich.''[34] Cells were treated with 1.5 mL of EBM-2 medium supplemented with 1 μM of peptides (QK, P1-QK, or P2-QK) or 2 nM recombinant human VEGF 165 (R&D Systems). Blank EBM-2 medium acted as negative control. Network formation was assessed at 24 h after cell seeding by immunofluorescence staining and confocal imaging ($n \geq 4$).

Immunofluorescent staining and imaging

Cells were fixed with 4% paraformaldehyde, permeabilized with 0.25% Triton X-100 solution in PBS, and blocked in 5% bovine serum albumin (BSA) and 0.5% Triton X-100 in PBS before incubation in anti-human VE-cadherin primary mouse antibody (1:200; Cell Signaling Technology). All antibodies are dissolved in 2.5% BSA and 0.5% Triton X-100 in PBS. After three washes, samples were further incubated with Alexa-488 anti-mouse antibody (1:1000; Life Technologies), rhodamine Phalloidin (1:300; Life Technologies), and DAPI (1 μg/mL; Life Technologies) before washing and mounting in ProLong Gold Antifade (Life Technologies). Images of cell morphology were obtained using a Leica TCS SP5 confocal microscope.

Spheroid outgrowth assay in three-dimensional collagen-fibronectin matrices

HUVEC spheroids consisting of about 500 cells per spheroid were generated in EBM-2 medium supplemented with 5% HI-FBS using AggreWell™ 400 plates (STEMCELL Technologies) following manufacturer's protocol. HUVEC spheroids were mixed with type I collagen (final concentration = 2 mg/mL) and fibronectin (final concentration = 5 μg/mL) in the EBM-2 medium with 5% HI-FBS. Polymerization was initiated by addition of NaOH solution (0.5 M initial concentration according to manufacturer's protocol), followed by transfer of 150 μL to individual wells in a 48-well plate and 30 min incubation at 37°C in a humidified incubator. Each matrix contained ~50 spheroids. The center of collagen matrix was hand injected with 30 μL of saline or MITCH with or without QK, P1-QK, or P2-QK (20 μM) using a 28G needle. After 10 min, 420 μL media was slowly added onto the collagen matrix to bring the total volume in the well to 600 μL. After 1 h, the media were replaced with fresh EBM-2 (5% HI-FBS) and the encapsulated spheroids were allowed to grow for 2 days. Spheroids were fixed, stained, and imaged as described previously. Confocal z-stack images were collected at ~3-μm intervals to a depth of ~100 μm into the collagen matrix using a 10× objective. Image stacks were compressed into a maximum projection image. The number of nuclei found outside of the compact spheroid boundary was manually counted ($n \geq 5$ for each group). Spheroid height was measured as the length observed along the z-axis from z-stack confocal images. The normalized outgrowth area was defined as the ratio of the projected cross-sectional area of all cells in the x-y plane to the cross-sectional area of the compact spheroid at day 2. Normalized outgrowth was quantified using Image J ($n \geq 5$).

Statistical analysis

Statistical analysis was performed using one-way analysis of variance followed by Tukey *post hoc* test. p-Value < 0.05 was considered statistically significant.

Results

Avidity increases the binding strength of P2 affinity tags relative to P1

Delayed release of P1-QK and P2-QK conjugates relative to QK is hypothesized to occur through specific interactions between the P1 or P2 affinity tag and C domains in MITCH. By linking two P1 domains with a tetraglycine spacer, we engineered P2 to have stronger interactions than P1 due to

avidity, or binding synergy from having multiple binding sites.[35] The tetraglycine spacer confers conformational flexibility but is hypothesized to be too short to allow both P domains to bind two C domains simultaneously. ITC was employed to evaluate these hypotheses (Supplementary Fig. S2). Fitting of ITC data with an independent-site model showed that binding enthalpy between C1 and P2 was 2.5× greater than that for C1 and P1 (Supplementary Table S1). Both P1 and P2 were determined to bind less than one C1 per molecule, suggesting that the two P domains within P2 are not simultaneously accessible. In multisite interactions, greater than additive increases in binding strength without changes in effective binding stoichiometry are a signature of avidity effects.[35]

Conjugation to P1 or P2 slows down QK release from MITCH by affinity immobilization

The effective diffusion coefficients of the peptide drug variants within MITCH were determined using FRAP. Fluorescently labeled QK, P1-QK, or P2-QK peptides were first homogenously incorporated within the MITCH matrix before a high-intensity laser was applied to photobleach a defined area within the gel. Diffusion of surrounding unbleached peptides into the bleached region results in characteristic fluorescence recovery profiles from which diffusivity constants of the peptides were derived.[32] Conjugation to P1 or P2 impeded the mobility of QK in MITCH, as apparent from the longer persistence of bleached regions

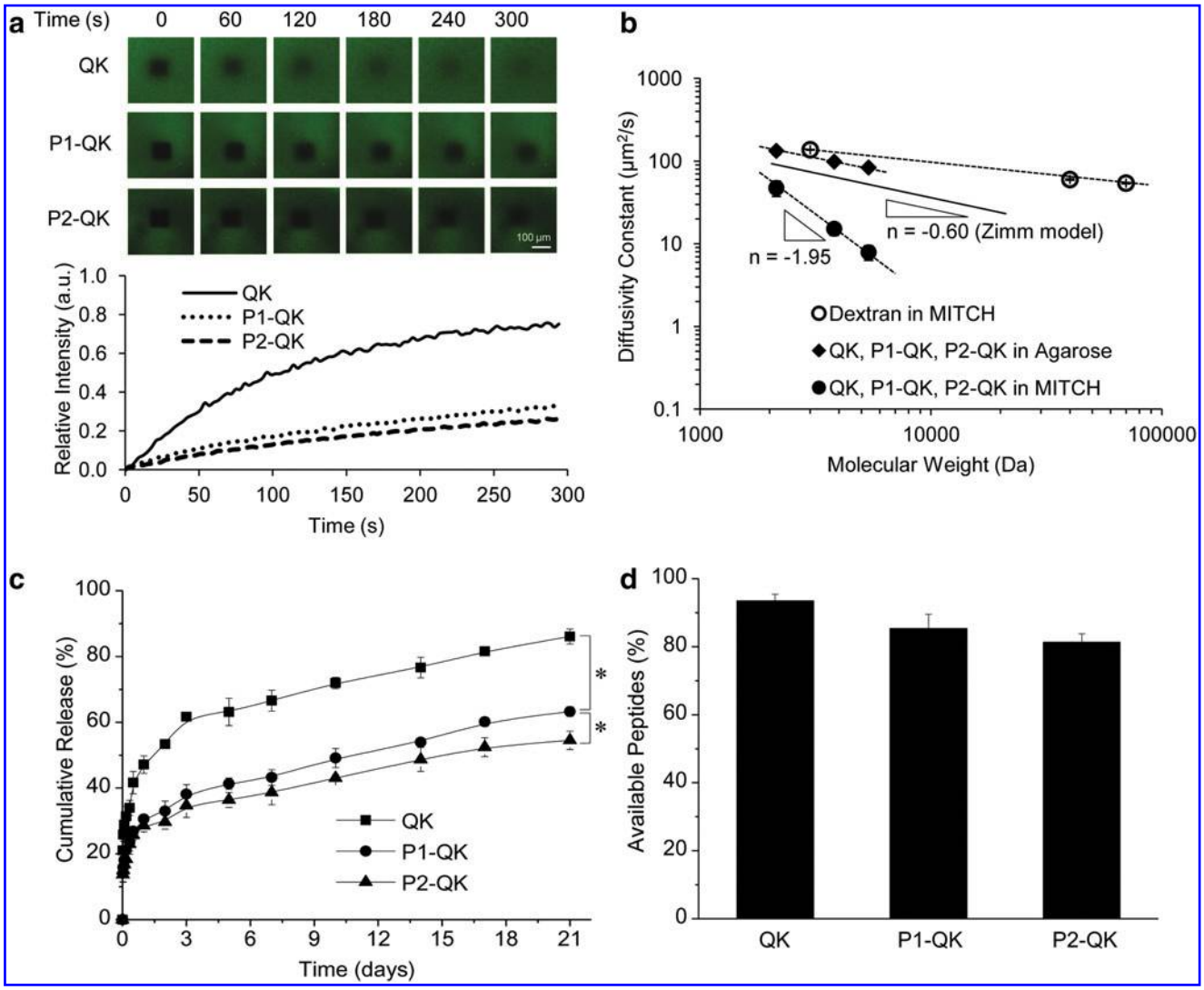

FIG. 2. Kinetics of encapsulated peptide drugs. **(a)** Fluorescence recovery after photobleaching (FRAP) characterization of diffusivity, showing time-lapse fluorescence images of photobleached areas (upper panel) and the corresponding fluorescence recovery curves (lower panel) used to derive diffusivity constants. **(b)** Relationship between diffusivity constant and molecular weight for the diffusion of peptide drugs in MITCH. Control systems, which do not include affinity immobilization, include diffusion of peptide drugs in agarose gels and diffusion of dextran molecules in MITCH. Solid line represents theoretical scaling for nonimmobilized molecules as predicted by the Zimm model. Diffusivity constants are listed in Table 1. **(c)** Cumulative amounts of peptide drugs released from MITCH into a bulk medium of phosphate buffered saline (PBS) (pH 7.4). $*p < 0.05$. **(d)** Cumulative amount of encapsulated peptide drug available for soluble release from MITCH. Color images available online at www.liebertpub.com/tea

Table 1. Diffusivity Constants of Peptide Drugs in MITCH or Agarose Gels, and of Dextran in MITCH

Peptide	*Molecular weight (Da)*	*Diffusivity in MITCH ($\mu m^2/s$)*[a]	*Diffusivity in agarose ($\mu m^2/s$)*[a]
QK	2139	47.4 ± 10.1	133.1 ± 13.2
P1-QK	3810	15.2 ± 2.6	98.5 ± 8.4
P2-QK	5368	7.9 ± 1.6	83.7 ± 4.9
	Molecular weight (Da)	*Diffusivity in MITCH ($\mu m^2/s$)*[b]	
Dextran	3000	137.3 ± 1.1	
	40000	59.9 ± 1.2	
	70000	54.2 ± 1.0	

[a]Determined through FRAP.
[b]Determined by fitting cumulative release curve to Fick's second law of diffusion from thin slabs (Supplementary Fig. S3).
MITCH, mixing-induced two-component hydrogel; FRAP, fluorescence recovery after photobleaching.

in the time-lapse images and the gentler slopes in the corresponding fluorescence recovery curves (Fig. 2a). Diffusivity constants obtained from FRAP analysis confirmed decreasing mobility from QK to P1-QK to P2-QK (Table 1).

FRAP experiments are material and time efficient, requiring 10 μL of sample volume and minutes of imaging time. As such, FRAP is a useful tool for studying molecular-level diffusion kinetics. The overall drug-release rate is a combination of both molecular-level diffusion kinetics, which occur on small time and length scales, and macro-diffusivity determinants, such as hydrogel swelling, hydrogel degradation, and initial burst release from the gel surface.[36] Therefore, bulk-release experiments that involve the submersion of peptide-containing MITCH in an aqueous medium and continuous sampling were performed in parallel. The cumulative release of QK, P1-QK, and P2-QK from bulk MITCH into PBS was consistent with the FRAP recovery and diffusivity trends (Fig. 2c), and displayed statistically significant difference from 2 h through 21 days of release. QK had the fastest rate of release, 86.1% over 21 days. In that same time, only 63.3% of P1-QK and 54.5% of P2-QK had been released. After disrupting the gel at day 21, the cumulative amount of encapsulated peptide available for soluble release was determined to be 93.5% for QK, 85.3% for P1-QK, and 81.4% for P2-QK (Fig. 2d), indicating that more soluble peptide was still entrapped in the MITCH gel and available for further release at even longer time points. The apparent loss of QK peptides may be due to insolubilization, degradation, or photobleaching of fluorescence. The ability of MITCH to retain peptides over several days is a promising first step toward addressing the short circulating half-lives of peptide drugs *in vivo*.

In addition to interactions with network backbone polymers, the molecular size of a macromolecule governs its diffusivity within a hydrogel.[37] To verify that specific interactions between P1-QK and P2-QK with MITCH are indeed the primary reason for their delayed release relative to QK, we devised two control delivery systems. In the first, we delivered the same three peptides from agarose gels in place of MITCH to verify immobilization by specific affinity. In the second, we kept the MITCH matrix constant and delivered dextran polymers of various molecular weights to control for molecular-size effects.

QK, P1-QK, and P2-QK are charged peptides with isoelectric points of 9.86, 9.16, and 6.84, respectively (Supplementary Table S1). Agarose gels are crosslinked networks of hydrophilic and electrically neutral polysaccharide chains. Hence, we anticipate QK, P1-QK, and P2-QK to be simply entrapped without adsorbing to the network backbone. FRAP experiments on QK, P1-QK, and P2-QK in 5% w/v agarose gels produced diffusivity constants that are higher than their respective values in MITCH (Table 1). In PBS (pH 7.4), QK carries a positive charge that nonspecifically interacts with negative charges on C7 and P9 in MITCH, whose isoelectric points are 4.26 and 3.38, respectively. As a result, QK alone has lower diffusivity in MITCH than in agarose. In contrast, P1-QK and P2-QK, which have progressively lower isoelectronic points and thus weaker electrostatic interactions to MITCH, continue to have further depression of diffusivity constants to values substantially lower than those in agarose. This supports the hypothesis of specific affinity immobilization of P1-QK and P2-QK to MITCH.

To assess contributions from molecular size, we conducted bulk-release experiments using neutral Texas Red dextran of different molecular weights as the cargo within MITCH. Dextrans are hydrophilic polysaccharides that are not expected to have specific affinity for the MITCH matrix. Hence, delayed release is primarily due to molecular-size effects dictated by simple Fickian diffusion through tortuous paths in the hydrogel mesh. Cumulative release curves of dextran (Supplementary Fig. S2) were fitted to Fick's second law of diffusion from thin slabs[33] to derive diffusivity constants (Table 1). All dextran samples, including the 70 largest kDa variant, were released faster than QK, the smallest of the peptides with a molecular weight of 2.1 kDa. This confirms that impedance of peptide mobility was a consequence of combined affinity immobilization and electrostatic interactions instead of molecular size.

We next employed a polymer physics approach to analyze the diffusivity constants and glean insights into the diffusion mechanisms for these three different systems. Diffusivity constant scales with molecular weight according to a power law $D = M^n$, where the exponent n is characteristic of diffusion mode.[38] In the diffusivity constant measurements, the peptide drugs were encapsulated at 0.4% w/v in both MITCH and agarose, and dextrans were encapsulated at 10 μM in MITCH. At such low concentrations, these macromolecules are expected to behave as polymers in the dilute regime. As such, their diffusion dynamics is described

by the Zimm model, where $n = -0.60$ for polymers diffusing in a good solvent.[39] On the logarithmic plot of diffusivity versus molecular weight (Fig. 2b), the Zimm-like scaling law was only obeyed by the control delivery systems, namely, peptide drugs in agarose gels and dextrans in MITCH. This validates our assumption of simple Fickian diffusion in these control systems. In contrast, with an n value of -1.95, peptide drugs in MITCH assumed a much more drastic decrease in diffusivity as molecular weight increased. This scaling relationship effectively approximates reptation dynamics in the entangled concentration regime, where n has a theoretical value of -2.[38] The fact that reptation-like kinetics was observed in the dilute regime provides further evidence of mobility impedance through affinity interactions as the peptides move within the MITCH network.

P1-QK and P2-QK conjugates maintain bioactive configurations and activate angiogenic signal transduction

The VEGF-mimetic activity of QK relies on the preservation of its α-helical structure, signified on a CD spectrum by pronounced double minima at 208 and 220 nm.[6] Binding to the pocket of C domain requires the P domain to fold into a left-handed polyproline II (PPII) helix, a conformation with a characteristic single negative peak at 200 nm on the CD spectrum.[40] P1-QK and P2-QK were created by modularly linking P and QK domains with tetraglycine spacers (Supplementary Fig. S1). In these conjugates, individual modules have to retain their native secondary structures in order to preserve function. CD spectroscopy, a powerful tool for structural comparison between peptide fusions and their parent peptides, revealed pure α-helix in QK and PPII helix in P1 and P2 (Supplementary Fig. S4). Linear combination of these elemental spectra can be used to deconvolute the CD readouts of P1-QK and P2-QK conjugates (Fig. 3a and Supplementary Fig. S4). Spectral addition of QK to P1 or P2 generated CD profiles that follow the corresponding P1-QK and P2-QK spectra, implying the preservation of individual helices in the conjugates. Based on this CD analysis, P1-QK and P2-QK conjugates are anticipated to behave as bifunctional peptides capable of specific binding to MITCH and VEGF-mimetic activation of angiogenic pathways.

The binding of VEGF to VEGF receptor 2 (VEGFR2) on endothelial cells leads to receptor dimerization and autophosphorylation. The phosphorylated VEGFR2 in turn initiates further cascades of protein phosphorylation, some of which promote cell survival, proliferation, and migration.[41–43] Derived from the helix sequence 17–25 of VEGF, QK has been reported to bind VEGF receptors and activate VEGFR2-mediated pathways.[6] To investigate whether conjugation to P1 or P2 abolishes QK's ability to initiate VEGFR2 signal transduction, we treated HUVECs with either P1-QK or P2-QK and used ELISA to quantify the extent of VEGFR2 phosphorylation in the cell. Relative to the blank media control, both P1-QK and P2-QK treatment groups showed elevated levels of phosphorylated VEGFR2 (Fig. 3b), consistent with previous findings.[6,28]

In VEGF-mediated angiogenesis, the ERK/MAPK cascade is the main mitogenic signaling pathway downstream of VEGFR2 activation.[43] To verify whether the activation of

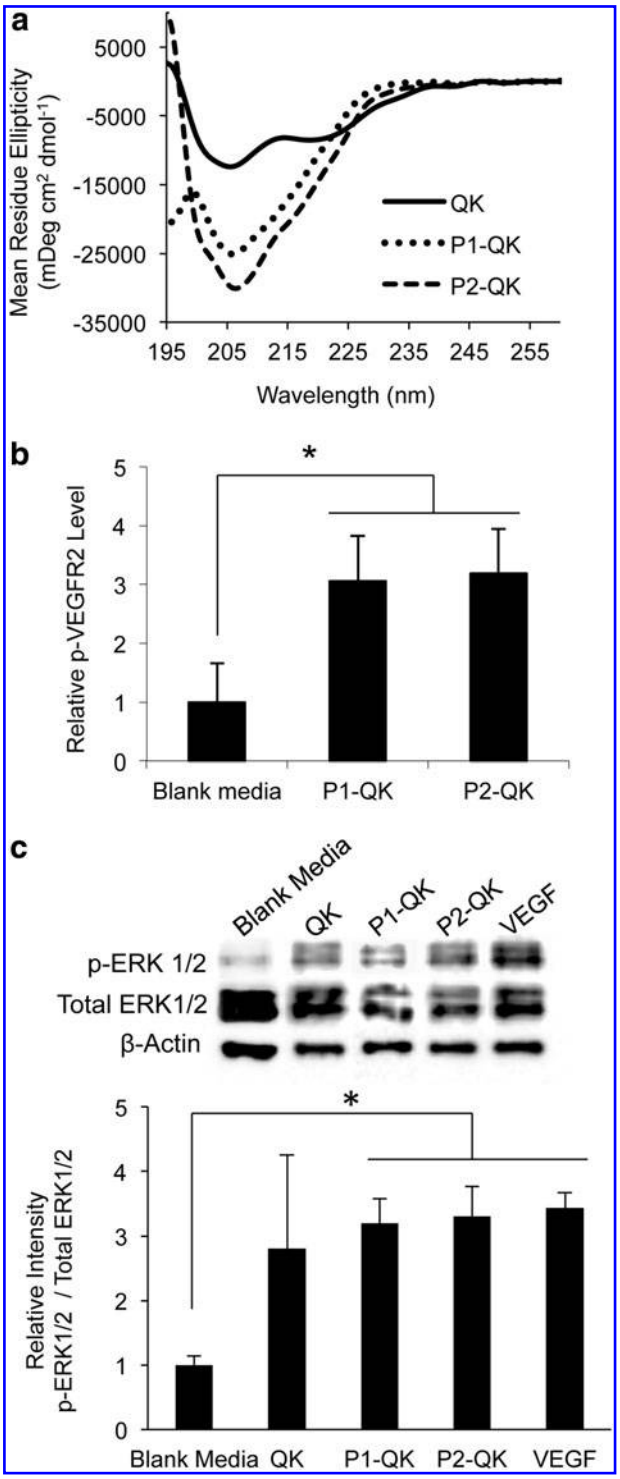

FIG. 3. Analyses of peptide drug bioactivity on endothelial cell signaling. **(a)** Circular dichroism spectra of QK, P1-QK, and P2-QK, demonstrating the α-helical structure requisite for angiogenic bioactivity (see Supplementary Fig. S4). **(b)** ELISA quantification of VEGFR2 receptor phosphorylation in human umbilical vein endothelial cells (HUVECs), following overnight serum starvation and 5-min incubation with 1 μM of soluble QK, P1-QK, or P2-QK, or 2 nM of soluble VEGF. **(c)** Western blotting of the cell proliferation signal phosphoERK1/2 in HUVECs, following overnight serum starvation and 15-min incubation with 1 μM of soluble QK, P1-QK, or P2-QK, or 2 nM of soluble VEGF. $*p < 0.05$.

VEGFR2 by P1-QK or P2-QK is further propagated into downstream angiogenic signals, we used western blotting to probe for the phosphorylation of ERK1/2 in HUVECs following treatment with the peptide drugs. Compared with blank media, treatment with QK, P1-QK, and P2-QK all induced significantly higher ERK1/2 phosphorylation, to a level similar to VEGF (Fig. 3c). Together, these data demonstrate the preservation of QK's ability to trigger VEGFR2 activation and the subsequent ERK/MAPK phosphorylation cascade, even when presented as a fusion to P1 or P2.

P1-QK and P2-QK activate endothelial cell migration and network formation

Once the VEGF pathway is activated, neovascularization proceeds through endothelial cell migration and proliferation to form capillary sprouts, followed by intercellular alignment into tubules with patent lumens.[44] The early morphogenetic events of EC migration and network formation can be mimicked *in vitro* to investigate specific cell functions.[34]

We performed *in vitro* scratch wound healing assays with HUVECs to assess the effects of P1-QK and P2-QK on endothelial cell migration, which is a critical step in new blood vessel formation.[43] HUVECs treated with the VEGF control showed fast wound closure (72.9% at 12 h) (Fig. 4a), consistent with previous reports of VEGF-mediated phosphorylation of VEGFR2 and ERK1/2 leading to cell proliferation and migration.[45] QK, P1-QK, and P2-QK also significantly promoted wound repair over blank media alone and achieved levels of wound closure (56.3%, 66.0%, and 62.0%, respectively) statistically similar to soluble VEGF.

Next, we sandwiched a monolayer of HUVECs between two layers of collagen matrix to assess the cells' capacity to form network-like structures upon treatment with QK peptides (Fig. 4b). Network-formation assays on soft matrices are reminiscent of vasculogenesis, the *de novo* creation of vascular-like networks from isolated endothelial cells.[34] After 24 h of culture in blank media without serum and growth factors, HUVECs maintained a confluent monolayer with typical cobblestone morphology, and VE cadherin staining revealed uniform cell–cell contact through adherens junctions. Within the same 24-h period, supplementing the media with QK, P1-QK, P2-QK, or VEGF resulted in cellular reorganization into network-like structures suggestive of early capillary formation.

In these scratch wound healing and network-formation assays, soluble forms of P1-QK and P2-QK were able to elicit EC phenotypic changes similar to those produced by QK and the parent VEGF protein, corroborating the angiogenic activities observed at the signal transduction level.

Injection of P1-QK- or P2-QK-releasing MITCH induces three-dimensional HUVEC outgrowth

To assess the activity of MITCH-delivered QK, P1-QK, and P2-QK on endothelial cells, we induced HUVEC outgrowth in three-dimensional (3D) matrices (Fig. 5a, b). HUVEC spheroids were encapsulated in a matrix of collagen type I and fibronectin previously reported to enable HUVEC invasion.[46] Next, drug-releasing MITCH was injected into the center of the matrix using a 28G needle. Media were changed 1 h post injection to mimic the *in vivo*

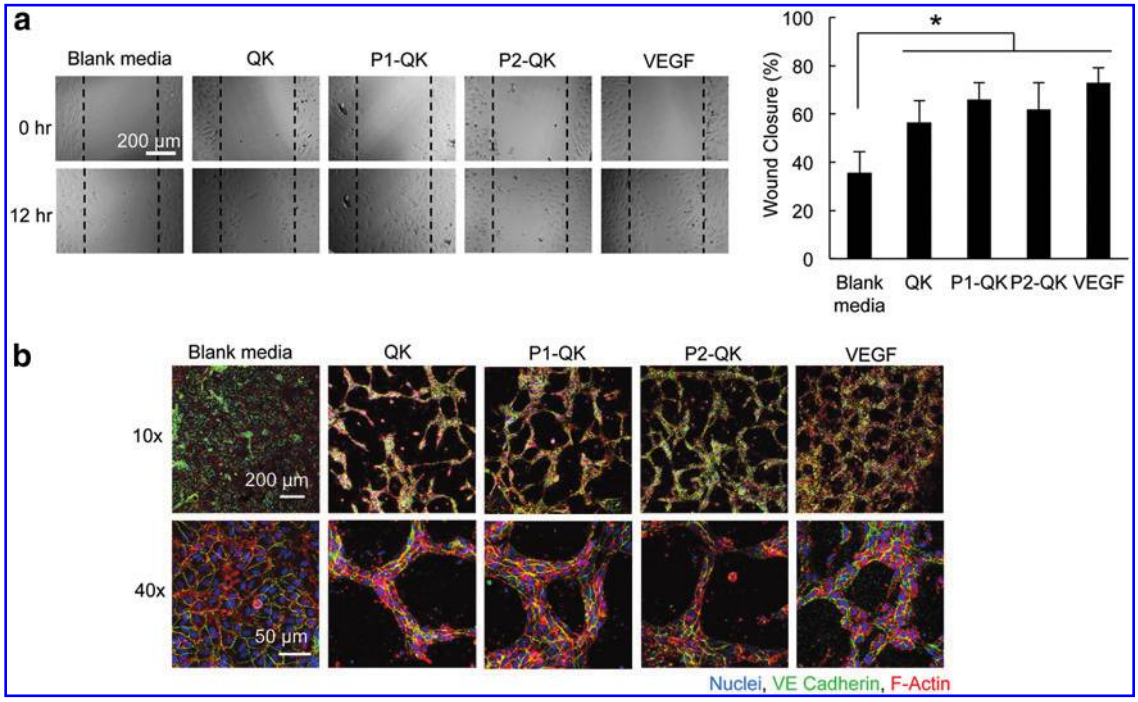

FIG. 4. *In vitro* stimulation of angiogenic cell phenotypes by peptide drugs. **(a)** Wound scratch assay measuring HUVEC proliferation and migration into wound area, assessed immediately and 12 h after wound creation and incubation with 1 μM of soluble QK, P1-QK, or P2-QK, or 2 nM of soluble VEGF. $*p < 0.05$. **(b)** *In vitro* tubulogenesis assay of HUVECs seeded between two collagen gels. Cell morphologies after 24 h of incubation with 1 μM of soluble QK, P1-QK, or P2-QK, or 2 nM of soluble VEGF were visualized by confocal microscopy. VEGF, vascular endothelial growth factor. Color images available online at www.liebertpub.com/tea

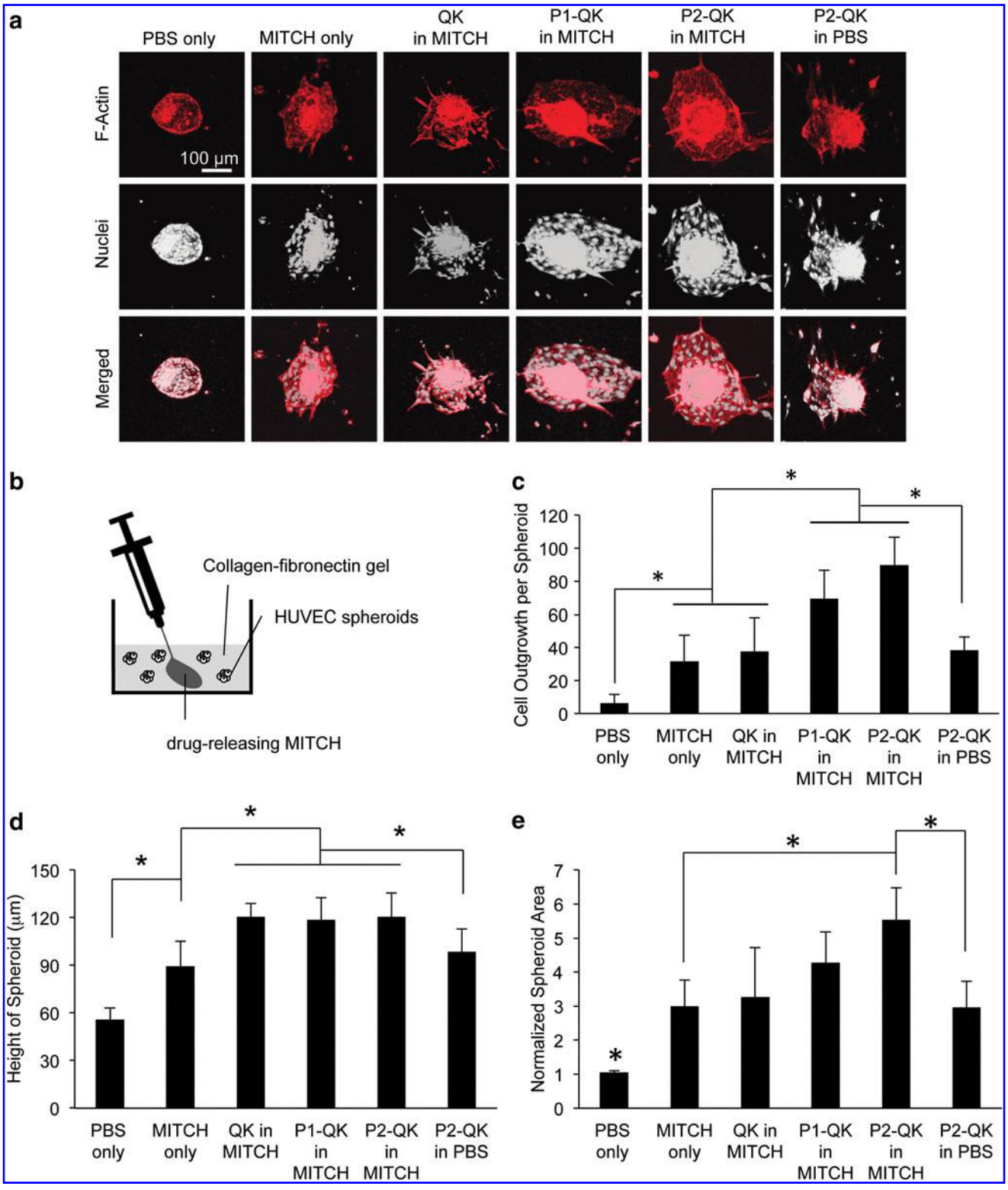

FIG. 5. Characterization and quantification of HUVEC spheroid outgrowth induced by MITCH-released peptide drugs in three-dimensional matrices at 2 days post injection. **(a)** Confocal maximum projection images of HUVEC spheroid outgrowth staining for F-actin (phalloidin, red, first row) and nuclei (Hoechst, white, second row), and a merge of two images (third row). Scale bar of 100 μm is applicable to all. **(b)** A scheme of injecting drug-releasing MITCH into matrices with HUVEC spheroids. Quantification of **(c)** number of cell outgrowth per spheroid, **(d)** height of spheroid (μm), and **(e)** normalized spheroid area at day 2 to the initially embedded spheroid; $n = 5$; $^*p < 0.05$. Color images available online at www.liebertpub.com/tea

effect of body fluid circulation and rapid attenuation of peptide drug concentration at therapy sites.[47]

In the negative control, the injection of PBS alone into the matrix resulted in minimal cell outgrowth (Fig. 5a, c). Injection of MITCH alone into the matrix supported a significant level of cell outgrowth from the spheroid compared to PBS alone, possibly due to the inclusion of RGD cell-adhesive ligands within MITCH. QK delivered from MITCH exhibited similar cell outgrowth as MITCH alone, implying that most of the QK peptide had been quickly released and diluted upon media exchange to a concentration insufficient to induce substantial cell migration. In contrast, both P1-QK and P2-QK delivered from MITCH stimulated significantly higher outgrowth than QK, suggesting that prolonged drug retention and slow release from MITCH were effective in sustaining high levels of QK activity even after the media exchange. In a control injection where P2-QK was delivered from PBS, cell outgrowth was similar to that for QK delivered from MITCH, suggesting that cells became depleted of the peptide drug once media were exchanged.

To confirm that HUVECs were stimulated to migrate in all directions within the 3D environment, we analyzed both the height of the spheroid along the *z*-axis and the projected cross-sectional area in the *x-y* plane (Fig. 5d, e). The height of spheroids treated with PBS alone was half of that stimulated by QK peptides delivered from MITCH. The latter also showed significantly higher values than P2-QK delivered from PBS. Similarly, P2-QK delivered from MITCH increased the projected area of spheroid outgrowth to a size significantly larger than treatment with MITCH alone or with P2-QK delivered from PBS. Both analyses demonstrate that QK peptides delivered from MITCH promoted 3D HUVEC outgrowth along all three axes. Taken together, these results suggest that QK peptides with affinity tags have prolonged residence time within MITCH, resulting in sustained local concentrations sufficient to induce 3D HUVEC outgrowth.

Discussion

We present a method of tuning the delivery kinetics of a VEGF-mimetic peptide by simple fusion to peptide domains that specifically bind to a protein-engineered hydrogel carrier. This delivery system is aimed toward plug-and-play simplicity and mix-and-match versatility. To this end, the hydrogel matrix was kept constant as an unmodified reservoir, while all design variables were imposed on the individual peptide drug payloads.

We harnessed molecular-recognition principles and modular peptide engineering to realize the design of this affinity-based delivery system. In MITCH, the crosslinking interactions between peptide domains in C7 and P9 are specific but reversible. Thus, these molecular-recognition domains could also act as docking sites for peptide conjugates bearing either a C or P affinity tag. P1-QK was designed to exploit this immobilization strategy. To bypass cloning and purification steps associated with recombinant synthesis, we employed the rapid and highly automated process of solid-phase peptide synthesis to make all the peptide drugs in our study. However, with the current synthesis limit of 70 amino acids, the total peptide length becomes a key design constraint. Therefore, the P domain became a natural choice as an affinity tag, as it is shorter than half the length of a C domain.

One way to tune release kinetics is by changing the affinity tag binding strength, which could be realized through a series of mutagenesis and library screening to identify a higher-affinity mutant.[48,49] While powerful, this directed evolution exercise is tedious. Instead, we increased binding strength by simply concatenating P1 to form P2, where the two P domains are linked by a short tetraglycine sequence. This approach was inspired by affinity augmentation through avidity, a classic strategy often employed in antibody engineering, where antibody fragments are multimerized to create high-affinity diabodies and triabodies.[50] Advantages arising from this simple P2 dimerization are threefold: (1) the resulting P2-QK conjugate is 53-amino-acid long (Supplementary Fig. S1), well within peptide synthesis capabilities; (2) binding energy was increased by more than double (Supplementary Fig. S2) without extensive mutagenesis and screening; and (3) the stoichiometric ratio of P2 binding to the C domain remained at 1:1, owing to the short tetraglycine linker sterically precluding two C domains from engaging both P domains in P2 at one time (Supplementary Table S1). These designed peptide drugs were readily encapsulated in MITCH, and molecular recognition of the affinity tags gave rise to significantly slower diffusivity and release kinetics of P2-QK relative to P1-QK and QK (Fig. 2).

In addition to simplicity and versatility, our approach offers further practical advantages for drug delivery. Drug encapsulation is achieved simultaneously as hydrogel formation through an easy, one-step mixing at nondenaturing physiological conditions (Fig. 1). Additionally, the drug-containing hydrogels are injectable (Fig. 5), thus allowing direct targeting to potential therapy sites without invasive surgical implantation.[26,27] Lastly, the purely proteinaceous nature of the system renders it biodegradable into natural amino acid products *in vivo*.[27]

Despite decades of research into the therapeutic potential of VEGF, clinical success following VEGF therapy has been limited. Bolus injections of recombinant human VEGF into ischemic tissues have produced off-target effects, such as lymphatic edema and abnormal vasculature formation, causing several human trials to be discontinued.[51] Later studies have found that optimal angiogenesis tends to ensue from a profile of high initial VEGF concentration followed by a gradual decrease over time.[52] Since VEGF has an intravenous half-life of 30 min *in vivo*,[53] this control is difficult to achieve. On top of delivery challenges, VEGF therapy poses practical barriers of cost-prohibitive manufacturing as well as storage and stability issues associated with full-length recombinant proteins.[54]

QK, a VEGF-mimetic peptide used in the current study, was developed to lower manufacturing costs, to facilitate ease of handling, and to improve stability relative to the full-length VEGF protein.[28] Following short initial bursts, QK conjugates were continuously released at nearly constant rates over several weeks *in vitro* (Fig. 2c). These results encourage future investigations into the angiogenic activity of the QK fusion peptide drugs *in vivo* and suggest the potential to engineer delivery kinetics that mimic the optimal VEGF-release profile.

The soluble P1-QK and P2-QK drug conjugates were able to activate VEGFR2 phosphorylation (Fig. 3b), stimulate ERK signal transduction (Fig. 3c), and induce HUVEC migration (Fig. 4a) and network formation (Fig. 4b). These results are consistent with previous findings where QK triggers the autophosphorylation of VEGFR2 intracellular domains, leading to the induction of HUVEC proliferation, survival, and migration.[6,28]

In vivo, drug availability in the microenvironment surrounding target cells has to be maintained in spite of continual depletion by interstitial fluid flow.[47] We attempted to simulate this *in vivo* scenario by creating a 3D construct where HUVEC spheroids were cultured in a collagen-fibronectin matrix and submerged in a bath of media. Direct injection of drug-releasing MITCH into the construct mimics the minimally invasive act of targeted delivery into a tissue (Fig. 5b). Media were exchanged shortly after injection to account for the replenishment of interstitial fluid. In this model, we demonstrated that P1-QK and P2-QK delivered from MITCH promoted extensive HUVEC spheroid outgrowth in all directions (Fig. 5). Such levels of outgrowth were not inducible by MITCH-delivered QK or saline-delivered P2-QK. These observations highlight the ability of MITCH to sustain the delivery of affinity-tagged QK peptides within time frames required for cellular remodeling.

Ultimately, tissue-level vascular regeneration is a complex process involving tightly regulated spatiotemporal coordination of multiple factors. The delivery of VEGF alone is known to produce leaky, immature, and poorly functioning vasculature.[55] Vessel stabilization and maturation requires smooth muscle cell and pericyte recruitment to newly formed capillaries, a process inducible by serial delivery of PDGF following VEGF.[56,57] Exploiting the distinct release kinetics of P1 and P2 conjugates to control the co-delivery of VEGF- and PDGF-mimetic peptides could be an extension of the current work.

The clinical relevance of multifactor therapy has motivated several modular, noncovalent delivery strategies. In these systems, the encapsulation and independent tuning of additional factors are typically accompanied by design modifications on the delivery carrier, requiring either new binding mediators with dissimilar affinities,[20,58,59] nano- and micro-particle incorporation,[56,60] or composite polymeric phases with differential physicochemical properties such as hydrophilicity.[61] These customized engineering steps may preclude easy translation to other biological systems.

Our approach of using affinity tag fusions to tune release kinetics enables truly modular and versatile adaptation to the delivery of other factors, as the fusions are made directly on individual payloads without modifying the MITCH carrier. Once the presence of an affinity tag has been confirmed to not interfere with drug activity, simple dimerization and avidity effects can be used to further increase the affinity tag binding strength. To the best of our knowledge, avidity effects have not been explored previously in biomaterial-assisted drug delivery strategies, and the use of avidity-controlled delivery could find broad application in other biomaterial systems for myriad regenerative medicine endeavors.

In summary, we presented a molecular-recognition strategy for tuning peptide delivery by affinity immobilization to an injectable protein-hydrogel system. A VEGF-mimetic peptide delivered using this strategy was slowly released at rates dictated by avidity-controlled immobilization strength, leading to sustained local concentrations that were able to induce VEGFR2-mediated endothelial cell migration and invasion. By virtue of component modularity, the system could be easily utilized for multifactor delivery, applicable not only to therapeutic angiogenesis, but also in other clinical models where temporal control of peptide drugs is critical.

Acknowledgments

W.M. was supported by a Stanford Graduate Fellowship and a Siebel Scholarship. This study was supported by grants from the NSF Career Award (DMR-0846363), the NIH TR01 (R01-DK085720) and New Innovator (DP2-OD006477), Genentech (1-PTD), and CIRM (RT2-01938). The authors thank Ruby Dewi for insightful scientific discussions and assistance with western blot, Kelly Huggins for CD spectroscopy training, Karen Dubbin for FRAP method optimization, and Kyle Lampe for advice on spheroid formation.

Disclosure Statement

No competing financial interests exist.

References

1. Vlieghe, P., Lisowski, V., Martinez, J., and Khrestchatisky, M. Synthetic therapeutic peptides: science and market. Drug Discov Today **15,** 40, 2010.
2. Craik, D.J., Fairlie, D.P., Liras, S., and Price, D. The future of peptide-based drugs. Chem Biol Drug Des **81,** 136, 2013.
3. Vanhee, P., *et al.* Computational design of peptide ligands. Trends Biotechnol **29,** 231, 2011.
4. Otvos, L., Jr. Peptide-based drug design: here and now. Methods Mol Biol **494,** 1, 2008.
5. Kumar, A., Voet, A., and Zhang, K.Y. Fragment based drug design: from experimental to computational approaches. Curr Med Chem **19,** 5128, 2012.
6. D'Andrea, L.D., *et al.* Targeting angiogenesis: structural characterization and biological properties of a *de novo* engineered VEGF mimicking peptide. Proc Natl Acad Sci USA **102,** 14215, 2005.
7. Lin, X., Takahashi, K., Liu, Y., Derrien, A., and Zamora, P.O. A synthetic, bioactive PDGF mimetic with binding to both alpha-PDGF and beta-PDGF receptors. Growth Factors **25,** 87, 2007.
8. LeSauteur, L., Wei, L., Gibbs, B.F., and Saragovi, H.U. Small peptide mimics of nerve growth factor bind TrkA receptors and affect biological responses. J Biol Chem **270,** 6564, 1995.
9. Xiao, J., *et al.* A small peptide mimetic of brain-derived neurotrophic factor promotes peripheral myelination. J Neurochem **125,** 386, 2013.
10. Nakamura, T., *et al.* Peptide mimics of epidermal growth factor (EGF) with antagonistic activity. J Biotechnol **116,** 211, 2005.
11. Tang, L., Persky, A.M., Hochhaus, G., and Meibohm, B. Pharmacokinetic aspects of biotechnology products. J Pharm Sci **93,** 2184, 2004.
12. Lipinski, C.A. Drug-like properties and the causes of poor solubility and poor permeability. J Pharmacol Toxicol Methods **44,** 235, 2000.

13. Harris, J.M., and Chess, R.B. Effect of pegylation on pharmaceuticals. Nat Rev Drug Discov **2,** 214, 2003.
14. Szlachcic, A., Zakrzewska, M., and Otlewski, J. Longer action means better drug: tuning up protein therapeutics. Biotechnol Adv **29,** 436, 2011.
15. Censi, R., Di Martino, P., Vermonden, T., and Hennink, W.E. Hydrogels for protein delivery in tissue engineering. J Control Release **161,** 680, 2012.
16. Katz, J.S., and Burdick, J.A. Hydrogel mediated delivery of trophic factors for neural repair. Wiley Interdiscip Rev Nanomed Nanobiotechnol **1,** 128, 2009.
17. Gonen-Wadmany, M., Goldshmid, R., and Seliktar, D. Biological and mechanical implications of PEGylating proteins into hydrogel biomaterials. Biomaterials **32,** 6025, 2011.
18. Veronese, F.M., and Mero, A. The impact of PEGylation on biological therapies. BioDrugs **22,** 315, 2008.
19. Lin, C.C., Boyer, P.D., Aimetti, A.A., and Anseth, K.S. Regulating MCP-1 diffusion in affinity hydrogels for enhancing immuno-isolation. J Control Release **142,** 384, 2010.
20. Wylie, R.G., *et al.* Spatially controlled simultaneous patterning of multiple growth factors in three-dimensional hydrogels. Nat Mater **10,** 799, 2011.
21. Nie, T., Akins, R.E., Jr., and Kiick, K.L. Production of heparin-containing hydrogels for modulating cell responses. Acta Biomater **5,** 865, 2009.
22. Sakiyama-Elbert, S.E., and Hubbell, J.A. Controlled release of nerve growth factor from a heparin-containing fibrin-based cell ingrowth matrix. J Control Release **69,** 149, 2000.
23. Sakiyama-Elbert, S.E., and Hubbell, J.A. Development of fibrin derivatives for controlled release of heparin-binding growth factors. J Control Release **65,** 389, 2000.
24. Wood, M.D., and Sakiyama-Elbert, S.E. Release rate controls biological activity of nerve growth factor released from fibrin matrices containing affinity-based delivery systems. J Biomed Mater Res A **84,** 300, 2008.
25. Wong Po Foo, C.T., Lee, J.S., Mulyasasmita, W., Parisi-Amon, A., and Heilshorn, S.C. Two-component protein-engineered physical hydrogels for cell encapsulation. Proc Natl Acad Sci USA **106,** 22067, 2009.
26. Mulyasasmita, W., Lee, J.S., and Heilshorn, S.C. Molecular-level engineering of protein physical hydrogels for predictive sol-gel phase behavior. Biomacromolecules **12,** 3406, 2011.
27. Parisi-Amon, A., Mulyasasmita, W., Chung, C., and Heilshorn, S.C. Protein-engineered injectable hydrogel to improve retention of transplanted adipose-derived stem cells. Adv Healthc Mater **2,** 428, 2013.
28. Finetti, F., *et al.* Functional and pharmacological characterization of a VEGF mimetic peptide on reparative angiogenesis. Biochem Pharmacol **84,** 303, 2012.
29. Lee, J.S., Wagoner Johnson, A.J., and Murphy, W.L. A modular, hydroxyapatite-binding version of vascular endothelial growth factor. Adv Mater **22,** 5494, 2010.
30. Chan, T.R., Stahl, P.J., and Yu, S.M. Matrix-bound VEGF mimetic peptides: design and endothelial-cell activation in collagen scaffolds. Adv Funct Mater **21,** 4252, 2011.
31. Koepsel, J.T., Nguyen, E.H., and Murphy, W.L. Differential effects of a soluble or immobilized VEGFR-binding peptide. Integr Biol **4,** 914, 2012.
32. Jonsson, P., Jonsson, M.P., Tegenfeldt, J.O., and Hook, F. A method improving the accuracy of fluorescence recovery after photobleaching analysis. Biophys J **95,** 5334, 2008.
33. Guo, Q., Knight, P.T., and Mather, P.T. Tailored drug release from biodegradable stent coatings based on hybrid polyurethanes. J Control Release **137,** 224, 2009.
34. Davis, J. Animal Models: A Practical Guide to Creating and Using Culture-Based Biomimetic Alternatives. Hoboken, NJ: Wiley-Blackwell, 2012.
35. Krishnamurthy, V.M., Estroff, L.A., and Whitesides, G.M. Multivalency in Ligand Design, in Fragment-based Approaches in Drug Discovery. Weinheim, FRG: Wiley-VCH Verlag GmbH & Co. KGaA, 2006.
36. Brandl, F., *et al.* Hydrogel-based drug delivery systems: comparison of drug diffusivity and release kinetics. J Control Release **142,** 221, 2010.
37. Hirota, N., Kumaki, Y., Narita, T., Gong, J.P., and Osada, Y. Effect of charge on protein diffusion in hydrogels. J Phys Chem B **104,** 9898, 2000.
38. de Gennes, P.G. Scaling Concepts in Polymer Physics. Ithaca, NY: Cornell University Press, 1979.
39. Colby, R.H. Dynamics in blends of long polymers with unentangled short chains. J Phys II **7,** 93, 1997.
40. Bochicchio, B., and Tamburro, A.M. Polyproline II structure in proteins: identification by chiroptical spectroscopies, stability, and functions. Chirality **14,** 782, 2002.
41. Olsson, A.K., Dimberg, A., Kreuger, J., and Claesson-Welsh, L. VEGF receptor signalling - in control of vascular function. Nat Rev Mol Cell Biol **7,** 359, 2006.
42. Zhang, Y., Furumura, M., and Morita, E. Distinct signaling pathways confer different vascular responses to VEGF 121 and VEGF 165. Growth Factors **26,** 125, 2008.
43. Munoz-Chapuli, R., Quesada, A.R., and Angel Medina, M. Angiogenesis and signal transduction in endothelial cells. Cell Mol Life Sci **61,** 2224, 2004.
44. Deroanne, C.F., Lapiere, C.M., and Nusgens, B.V. *In vitro* tubulogenesis of endothelial cells by relaxation of the coupling extracellular matrix-cytoskeleton. Cardiovasc Res **49,** 647, 2001.
45. Swendeman, S., *et al.* VEGF-A stimulates ADAM17-dependent shedding of VEGFR2 and crosstalk between VEGFR2 and ERK signaling. Circ Res **103,** 916, 2008.
46. Shamloo, A., and Heilshorn, S.C. Matrix density mediates polarization and lumen formation of endothelial sprouts in VEGF gradients. Lab Chip **10,** 3061, 2010.
47. Lin, J.H., and Lu, A.Y. Role of pharmacokinetics and metabolism in drug discovery and development. Pharmacol Rev **49,** 403, 1997.
48. Dalby, P.A., Hoess, R.H., and DeGrado, W.F. Evolution of binding affinity in a WW domain probed by phage display. Protein Sci **9,** 2366, 2000.
49. Yaffe, M.B., and Smerdon, S.J. The use of *in vitro* peptide-library screens in the analysis of phosphoserine/threonine-binding domain structure and function. Annu Rev Biophys Biomol Struct **33,** 225, 2004.
50. Kortt, A.A., Dolezal, O., Power, B.E., and Hudson, P.J. Dimeric and trimeric antibodies: high avidity scFvs for cancer targeting. Biomol Eng **18,** 95, 2001.
51. Lei, Y., Haider, H., Shujia, J., and Sim, E.S. Therapeutic angiogenesis. Devising new strategies based on past experiences. Basic Res Cardiol **99,** 121, 2004.
52. Silva, E.A., and Mooney, D.J. Effects of VEGF temporal and spatial presentation on angiogenesis. Biomaterials **31,** 1235, 2010.
53. Eppler, S.M., *et al.* A target-mediated model to describe the pharmacokinetics and hemodynamic effects of recombinant

human vascular endothelial growth factor in humans. Clin Pharmacol Ther **72,** 20, 2002.
54. Dranitsaris, G., Amir, E., and Dorward, K. Biosimilars of biological drug therapies: regulatory, clinical and commercial considerations. Drugs **71,** 1527, 2011.
55. Yancopoulos, G.D., *et al.* Vascular-specific growth factors and blood vessel formation. Nature **407,** 242, 2000.
56. Richardson, T.P., Peters, M.C., Ennett, A.B., and Mooney, D.J. Polymeric system for dual growth factor delivery. Nat Biotechnol **19,** 1029, 2001.
57. Chen, R.R., Silva, E.A., Yuen, W.W., and Mooney, D.J. Spatio-temporal VEGF and PDGF delivery patterns blood vessel formation and maturation. Pharm Res **24,** 258, 2007.
58. Freeman, I., and Cohen, S. The influence of the sequential delivery of angiogenic factors from affinity-binding alginate scaffolds on vascularization. Biomaterials **30,** 2122, 2009.
59. Lin, C.C., and Metters, A.T. Bifunctional monolithic affinity hydrogels for dual-protein delivery. Biomacromolecules **9,** 789, 2008.
60. Kim, S., *et al.* Sequential delivery of BMP-2 and IGF-1 using a chitosan gel with gelatin microspheres enhances early osteoblastic differentiation. Acta Biomater **8,** 1768, 2012.
61. Xu, W., Atala, A., Yoo, J.J., and Lee, S.J. Controllable dual protein delivery through electrospun fibrous scaffolds with different hydrophilicities. Biomed Mater **8,** 014104, 2013.

Address correspondence to:
Sarah C. Heilshorn, PhD
Department of Materials Science and Engineering
476 Lomita Mall, McCullough Room 246
Stanford University
Stanford, CA 94305-4045

E-mail: heilshorn@stanford.edu

Received: June 19, 2013
Accepted: December 4, 2013
Online Publication Date: January 30, 2014